sensors

MDPI

Article

Characterization of Shear Horizontal Waves Using a 1D Laser Doppler Vibrometer

Alaa Elhady and Eihab M. Abdel-Rahman *

Department of System Design Engineering, University of Waterloo, Waterloo, ON N2L 3G1, Canada; alaaeldin.ahmed@edu.uwaterloo.ca
* Correspondence: eihab@uwaterloo.ca

Abstract: We developed a new technique for the detection of shear horizontal surface acoustic waves (SH-SAW) using a one-dimensional laser-based Doppler vibrometer. It measures the out-of-plane surface deformation at the fingertip of an interdigitated transducer (the boundary of the wave aperture) and uses it to estimate the instantaneous in-plane displacement field given the substrate Poisson ratio. It can also estimate the degree of surface confinement (wave decay rate). The proposed approach was first verified using finite element analysis (FEA) and demonstrated experimentally using a Bleustein–Gulyaev resonator.

Keywords: SH waves; Bleustein–Gulyaev waves; vibrometer; SAW detection; MEMS characterization

check for updates

Citation: Elhady, A.; Abdel-Rahman, E.M. Characterization of Shear Horizontal Waves Using a 1D Laser Doppler Vibrometer. *Sensors* **2021**, *21*, 2467. https://doi.org/10.3390/s21072467

Academic Editor: Steve Vanlanduit

Received: 12 March 2021
Accepted: 29 March 2021
Published: 2 April 2021

Publisher's Note: MDPI stays neutral with regard to jurisdictional claims in published maps and institutional affiliations.

Copyright: © 2021 by the authors. Licensee MDPI, Basel, Switzerland. This article is an open access article distributed under the terms and conditions of the Creative Commons Attribution (CC BY) license (https://creativecommons.org/licenses/by/4.0/).

1. Introduction

Surface acoustic waves (SAWs) propagating in piezoelectric materials have numerous applications, such as in sensors [1–3], actuators [4,5], filters [6–8], delay lines [9], and radio-frequency identification applications [10,11]. They are usually excited via a set of interdigitated electrodes (IDTs) that are deployed as transmitters and receivers or as non-collocated [12,13] or collocated [14] transceivers. Resonant transceivers create standing waves by trapping the waves using reflectors made of another set of IDTs [14] or an acoustic impedance mismatch, such as deep grooves [15].

Characterization of these waves is integral to SAW technology and research. A common method for SAW characterization is the use of Laser Doppler Vibrometry (LDV) to measure out-of-plane vibrations [16,17]. This allows for the accurate evaluation of the frequency response of SAW resonators, which is essential in filter design. However, shear horizontal surface acoustic waves (SH-SAWs) [18] often exhibit no out-of-plane components within the wave aperture, and thus require unconventional detection approaches. Shear horizontal (SH) waves, such as Bleustein–Gulyaev waves (BGWs) [19,20], are attractive in filter design [21,22], since they often offer higher quality factors, as well as in other applications [3,7,23].

For SAW devices based on semi-transparent substrates, such as lithium tantalate, one approach involves passing a laser beam through the material and observing polarization changes due to shear strain [24]. However, this method does not apply to opaque substrates or those covered with opaque films.

Another approach is to place the substrate at a tilted orientation with respect to the incident laser beam [25,26]. In this case, the beam must land on the edge of a structure erected on the piezoelectric substrate. This allows the in-plane vibration to be detected through LDV. However, the tilt angle creates challenges that increase the complexity of the experimental setup. It is also not applicable for SAWs that have few or no erect structures on the substrate surface, except for the IDT. However, the IDT thickness is usually in the sub-micrometer scale [27,28], which is small in comparison with the laser beam spot size.

Another procedure involves using multiple simultaneous laser beams [29,30], which land at different angles with respect to the substrate in order to capture both in-plane and

out-of-plane motions. A similar technique utilizes a single laser beam, but changes the angle of the substrate mechanically [31]. These techniques form the basis of specialized 2D and 3D vibrometry, but come at a significantly increased experimental setup complexity and cost.

More common approaches to full-field capture rely on fast cameras [32] and 3D digital image correlation (3D-DIC) [33]. The images are analyzed to detect in-plane motion, and thus, high-speed cameras are required in high-frequency applications. This usually inflates the complexity and cost of 3D-DIC and is limited in frequency by the frame rate of the camera used.

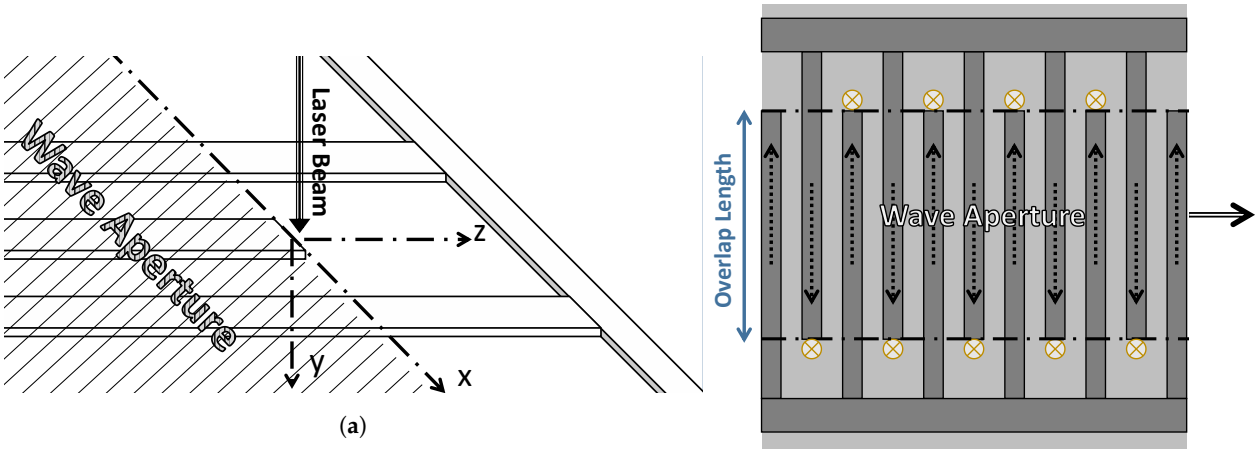
In this paper, we present a novel approach to detecting SH-SAWs using traditional 1D vibrometers that are applicable to high-frequency SH-SAW-based devices. The proposed technique is first explained, and then finite element analysis (FEA) is used for initial verification. Finally, experimental validation is presented by detecting an SH-SAW, namely a BGW.

2. Proposed Technique

SH waves propagate within the aperture, which is set by the dimensions of the IDTs. The aperture of the wave is confined to the area where the IDT fingers overlap. Typically, the overlap length is assumed to be large enough for the wave to be considered invariant along that direction. Beyond this aperture, the behavior is usually not of interest to researchers and engineers.

However, just outside of the wave aperture, at the fingertip, there is an area that can be of great value. SH waves act as a boundary load on this area and result in out-of-plane surface strains and deformations. Since this deformation is directly related to the SH wave's time history, it is ripe for exploitation as a measure of the SH wave. We propose the use of LDV to measure those deformations by using an incident laser beam focused on this area.

Figure 1a shows a schematic of the proposed experimental configuration. The origin of the coordinate system is taken on the surface of the substrate directly below the intersection of the finger's mid-line and its tip. The wave propagates along the x-axis, creating a displacement field $u(x, y, z, t)$ along the z-axis. A laser beam that is incident along the y-axis is used to measure the out-of-plane surface deformation $w(0, 0, z_\circ, t)$ at the point on the z-axis where the deformation reaches a maximum.



(**a**) (**b**)

Figure 1. (**a**) The experimental configuration of the proposed measurement technique. (**b**) Positions of the laser spot (marked by ⊗), the displacement field $u(x, y, z, t)$ (marked by the dashed-line arrows), and the propagation direction of the shear horizontal (SH) wave (marked by the double-line arrow).

Figure 1b shows the top view of the IDT, the SH wave, and the allowable locations of the laser beam spot on the substrate. Any of those positions can be used in the proposed

detection scheme. To characterize the displacement field $u(x, y, z, t)$, we need to identify a relationship between the time history of the measurement signal $w_\circ(t) = w(0, 0, z_\circ, t)$ and the instantaneous amplitude of the shear wave $u_\circ(t)$. We hypothesize the existence of a constant relationship such that $\alpha = w_\circ / u_\circ$. The FEA software COMSOL was used to test the validity of this hypothesis and to estimate α.

3. FEA

The region under study was a cuboid sector of the substrate bounded by the fingertip and the substrate edge (Figure 2). The distance between those boundaries was on the order of L = 2 mm. The finger width was w_d = 10 µm and the total width of the region under study was $2w_d$, with a margin of $\frac{1}{2}w_d$ on either side of the finger. The substrate was made of Navy Type I Lead Zirconate Titanate I (PZT4) with a Young's modulus of $E = 63$ GPa and a Poisson ratio of $\nu = 0.32$. The thickness was set to $H = 3$ mm to match that of the fabricated substrate. This region was meshed in the Finite Element Model (FEM) using 60,344 tetrahedral elements with 20,230 mesh vertices.

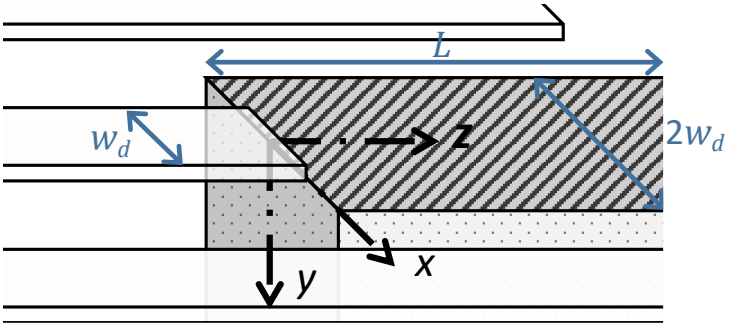


Figure 2. Interdigitated electrode (IDT) fingers and the piezoelectric substrate. The highlighted section represents the sector under study.

By assuming a wave frequency that is away from structural resonances of the sector under study, we could analyze its quasi-static response under the in-plane displacement:

$$u(x, y, 0) = u_\circ e^{-\frac{\pi}{\lambda r} y}; \qquad -\frac{1}{2}w_d \le x \le \frac{1}{2}w_d \;\; \& \;\; 0 \le y \le H. \tag{1}$$

This was applied by the finger to the left face $(z = 0)$ of the sector, where $u_\circ = u_\circ(t)$ is the instantaneous value of the displacement field at the fingertip, λ is the wavelength, and r is the wave decay rate. To preclude rigid body motions, the bottom plane of the substrate was held fixed at $u(x, H, z) = 0$, while the substrate faces at $y = 0$, $x = \pm w_d$, and $z = L$ were left free.

Figure 3 shows the resulting surface deformation under compressive (positive) and tensile (negative) prescribed in-plane displacements of $u_\circ = \pm 100$ nm, where the wavelength and decay rate were set to $\lambda = 40$ µm and $r = 1$. Varying the prescribed displacement $u_\circ$ within this range, the relationship between $u_\circ$ and the peak surface deformation $w_\circ = w(0, 0, z_\circ)$ was found to be linear.

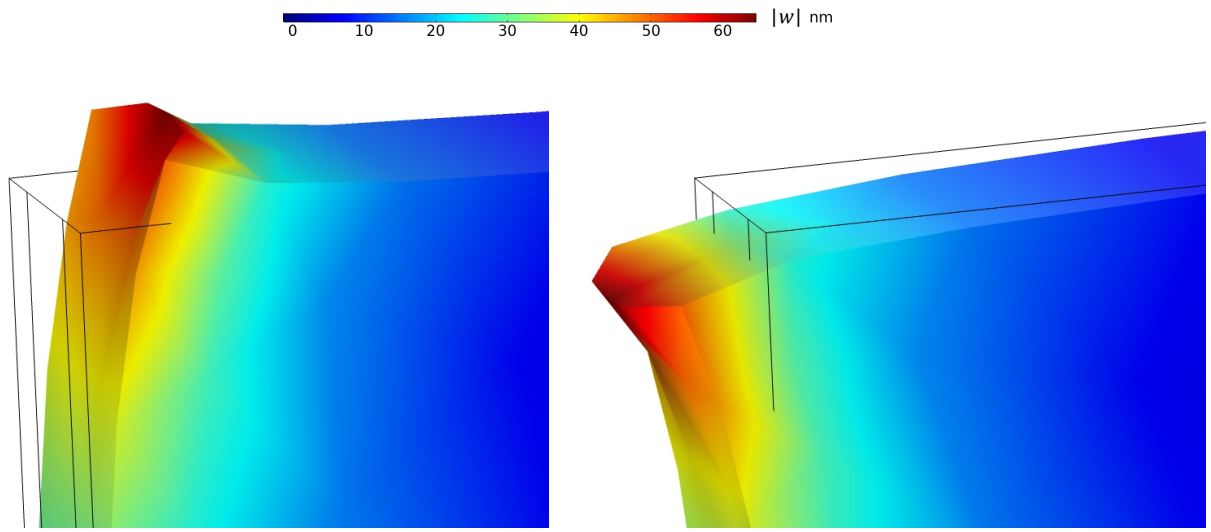


Figure 3. Finite element analysis (FEA) of the deformation under (**a**) positive and (**b**) negative in-plane displacement, u.

We investigated the variation in the surface deformation along the mid-line of the finger (z-axis) beyond the tip $w(0,0,z)$ in order to determine the maximum point's offset distance from the fingertip $z_\circ$ and, therefore, the optimal location of the laser spot. Figure 4 shows $w(0,0,z)$ normalized with respect to the maximum in-plane displacement $u_\circ$. The out-of-plane displacement decays exponentially away from the fingertip, and therefore, the optimum position to place the laser beam is at the fingertip with $z_\circ = u_\circ$.

Most SH waves have sub-micron shear displacements, while the LDV laser spot is typically between 1 and 10 µm. Therefore, the translation of the fingertip would not interrupt measurement, and the laser spot can keep the optimal point $z_\circ$ within focus. However, achieving optimal positioning would require an infinitesimal spot size. Since the spot size is finite and the deformation field decays exponentially, we propose the location of the spot in direct "contact" with the fingertip.

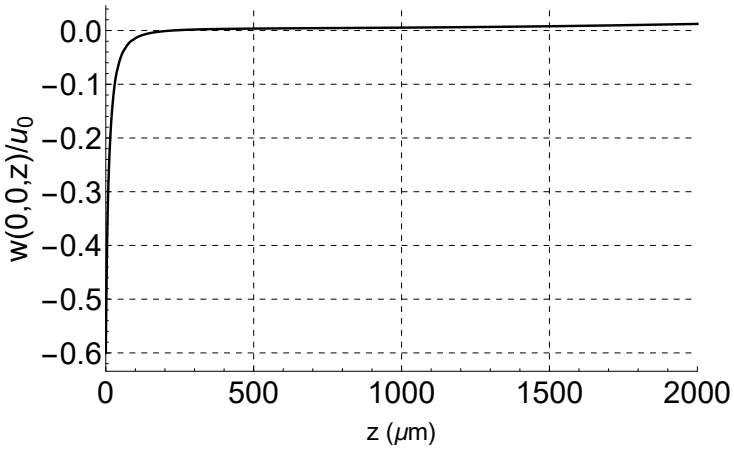


Figure 4. The normalized surface deformation simulated by COMSOL.

The decay rate of the deformation field depends on the type of SH-SAW, the substrate properties, and the boundary conditions. This rate determines the degree of the SH wave's localization to the substrate surface. To determine whether variation in the decay rate may impose further limits on the proposed experimental technique, we compare in Figure 5 the normalized deformation along the fingertip mid-line $w(0,0,z)/u_\circ$ for a range (r = 1–100) of decay rates. It was found that the surface deformation resulting from less-confined shear waves decays at a slower rate. For $r = 100$, the surface deformation drops to half value at

$z = 370\,\mu$m, which is marked with an asterisk in Figure 5. The linear relationship between the peak in-plane displacement $u_\circ$ and the peak surface deformation $w_\circ$ also changes from $w_\circ = -0.6u_\circ$ at $r = 1$ to $w_\circ = -0.4u_\circ$ at $r = 100$. Highly confined surface waves exhibit a higher deformation ratio α, but require a smaller laser spot.

As expected, the relationship between in-plane displacement and out-of-plane deformation was found to be independent of Young's modulus and linearly dependent on Poisson's ratio. Specifically and for a decay rate of $r = 1$, the deformation ratio varied from $\alpha = -0.45$ for $\nu = 0.1$ to $\alpha = -0.63$ for $\nu = 0.5$.

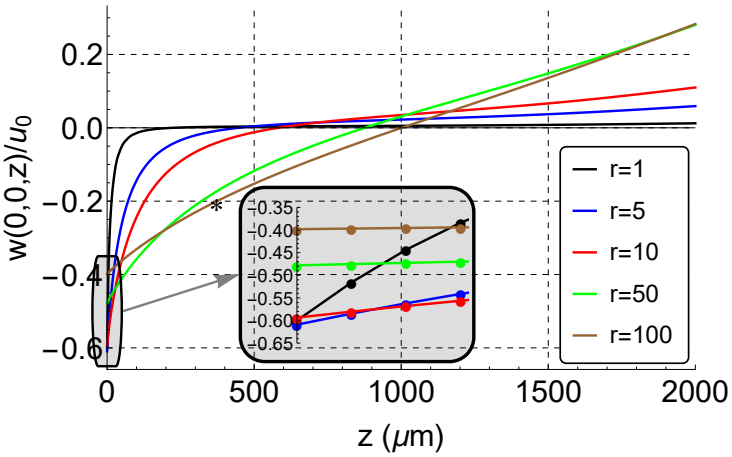


Figure 5. Variation in the normalized surface deformation as a function of surface wave confinement.

4. Experimental Validation

The proposed technique was deployed to characterize BGWs. Such waves [19,20] propagate exclusively on the surface of shear-poled piezoelectric materials. They are composed of a shear displacement field $u(x, y, z)$ along the z-direction (Figure 1a) coupled to an electromagnetic field propagating in the x-direction. BGWs have been used in telecommunication filters [7] and viscosity sensors [34–37].

A 64 MHz BGW resonator was designed and fabricated by patterning an IDT on the surface of a shear-poled PZT4 substrate. The width of the fingers was set to 10 μm, corresponding to a wavelength of $\lambda = 40\,\mu$m. The IDTs were fabricated on a polished and shear-poled PZT4 substrate. Using physical vapor deposition, a 400 nm thick aluminum layer was sputtered onto the substrate. A positive photoresist (Shipley 1811) was spun onto the substrate, baked, patterned using lithography, and developed using MF-319. Finally, an aluminum etchant was used to etch the aluminum layer into the desired electrode pattern, and the photoresist was stripped. Figure 6 shows the fabricated resonator under the microscope.

The behavior of BGWs in PZT4 is well documented [7,38]. The response to a potential field imposed by applying voltage waveform $V(t)$ to the substrate surface via an IDT is the displacement field [39]:

$$u_\circ(t) = d_{15}V(t), \tag{2}$$

where $d_{15} = 0.496$ nm/V [38] is the shear stress piezoelectric constant. This relationship can be expressed in terms of the measured out-of-plane deformation as:

$$w_\circ(t) = 0.496\alpha V(t)(\text{nm}). \tag{3}$$

The resonator was placed under the microscope-based Polytech MSA-600 Laser Doppler Vibrometer. Direct probing of the IDT under the microscope was employed to supply the drive voltage $V(t)$. BGWs were excited quasi-statically via a ramp waveform with a frequency of 30 kHz—far away from resonance—using a B&K Precision-4054 function generator.

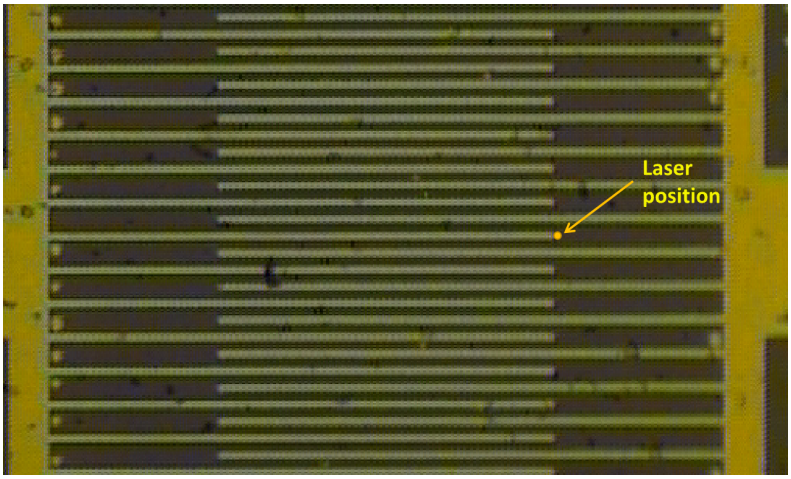


Figure 6. A microscopic image of the fabricated Bleustein–Gulyaev wave (BGW) IDT showing the location of the Laser Doppler Vibrometry (LDV) laser spot.

5. Results and Discussion

The LDV laser beam spot was located directly in front of the fingertip (Figure 6). The measured response to the rising side of the ramp was averaged 30 times. Figure 7 compares the experimental results (black circles) to the values predicted by Equation (3) (blue line), where the displacement ratio was set to $\alpha = -0.56$.

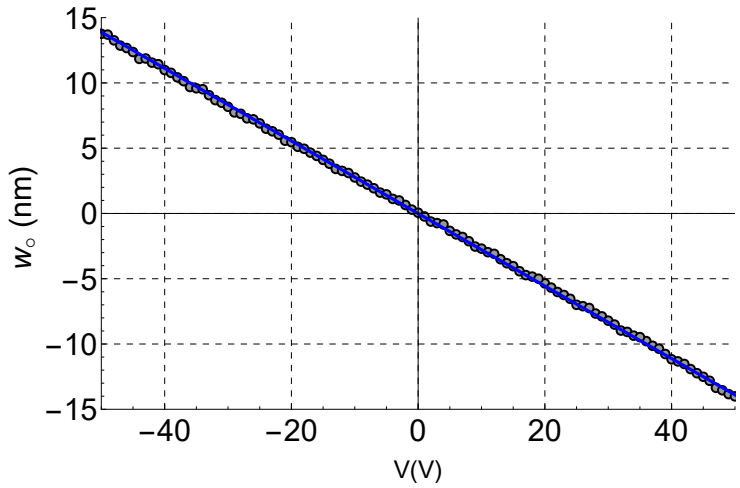


Figure 7. Experimental validation for the proposed technique. Experimental measurements are shown as black circles, and the model prediction line is shown as a solid blue line.

Assuming that the vibrometer-measured displacement represents the average surface deformation within the field illuminated by the spot, Figure 5 can be used to estimate the decay rate r given the spot size. In our case, the laser beam spot size was measured as 9 µm. An FEM simulation was then employed to identify the decay rate r, where the average of the deformation ratio α over the initial 9 µm along the z-axis was the same as that evaluated experimentally. It was found to be $r = 10$. This is reasonable considering that the metallization of the IDT enhances the confinement of the wave to the substrate surface [40].

The relationship between displacement and applied voltage was found to be linear for PZT4, as shown in Figure 7. This is in agreement with the literature on the small-displacement response of piezoelectric materials [41], thereby further validating the proposed technique. It is also in agreement with the linear relationship (Equation (3)) predicted through FEA.

The proposed technique can, therefore, be used to characterize the instantaneous amplitude of the shear displacement $u_\circ(t)$ of SH-SAWs. It can also be used to estimate wave confinement r to the surface. As a result, it can be used to characterize the time history and frequency response of SH-wave-based sensors and actuators. However, the excitation frequency must be restricted to a frequency range away from the resonances of the substrate sector in front of the fingertip. This restriction does not represent an onerous limitation, since those resonances occur in a much higher frequency range than resonances of the IDT due to the respective sizes of the IDT and the sector.

Moreover, once the displacement ratio α has been determined under forced excitation conditions, away from the IDT resonances, the IDT can be excited at resonance in order to determine its frequency response and identify its quality factor. The quality factor can be calculated as the ratio of the response at resonance to the static response or using the half-power bandwidth method.

6. Conclusions

We developed a novel technique that uses a 1D Laser Doppler Vibrometer to detect and characterize shear horizontal surface acoustic waves (SH-SAWs). The technique exploits the out-of-plane deformation appearing on the boundaries of the wave aperture as it propagates within. The proposed method was analyzed using a finite element model and validated experimentally using a Bleustein–Gulyaev resonator. It was successful in estimating the in-plane displacement field and the wave decay rate. This technique, therefore, provides researchers with a quick and effective method for characterizing SH-SAWs.

Author Contributions: Conceptualization, visualization, validation, and draft writing A.E.; investigation and methodology, A.E. and E.M.A.-R.; manuscript revision and supervision, E.M.A.-R. All authors have read and agreed to the published version of the manuscript.

Funding: This research received no external funding.

Institutional Review Board Statement: Not applicable.

Informed Consent Statement: Not applicable.

Data Availability Statement: The data that support the findings of this study are available from the corresponding author upon reasonable request.

Conflicts of Interest: The authors declare no conflict of interest.

References

1. Bo, L.; Xiao, C.; Hualin, C.; Mohammad, M.A.; Xiangguang, T.; Luqi, T.; Yi, Y.; Tianling, R. Surface acoustic wave devices for sensor applications. *J. Semicond.* **2016**, *37*, 021001.
2. Devkota, J.; Ohodnicki, P.R.; Greve, D.W. SAW sensors for chemical vapors and gases. *Sensors* **2017**, *17*, 801. [CrossRef]
3. Zhang, C.; Caron, J.J.; Vetelino, J.F. The Bleustein–Gulyaev wave for liquid sensing applications. *Sens. Actuators B Chem.* **2001**, *76*, 64–68. [CrossRef]
4. Kurosawa, M.; Takahashi, M.; Higuchi, T. Ultrasonic linear motor using surface acoustic waves. *IEEE Trans. Ultrason. Ferroelectr. Freq. Control* **1996**, *43*, 901–906. [CrossRef]
5. Shigematsu, T.; Kurosawa, M.K. Miniaturized SAW motor with 100 MHz drive frequency. *IEEJ Trans. Sens. Micromach.* **2006**, *126*, 166–167. [CrossRef]
6. Matthews, H. Surface wave filters: Design, construction, and use. *Proc. IEEE* **1977**, *67*, 1086–1087.
7. Kadota, M.; Ago, J.; Horiuchi, H. A Bleustein-Gulyaev-Shimizu wave resonator having resonances for TV and VCR traps. *IEEE Trans. Microw. Theory Tech.* **1996**, *44*, 2758–2762. [CrossRef]
8. Morgan, D. *Surface Acoustic Wave Filters: With Applications to Electronic Communications and Signal Processing*; Academic Press: Cambridge, MA, USA, 2010.
9. Schulz, M.; Holland, M. Surface acoustic wave delay lines with small temperature coefficient. *Proc. IEEE* **1970**, *58*, 1361–1362. [CrossRef]
10. Harma, S.; Arthur, W.G.; Hartmann, C.S.; Maev, R.G.; Plessky, V.P. Inline SAW RFID tag using time position and phase encoding. *IEEE Trans. Ultrason. Ferroelectr. Freq. Control* **2008**, *55*, 1840–1846. [CrossRef] [PubMed]

11. Wei, L.; Tao, H.; Yongan, S. Surface acoustic wave based radio frequency identification tags. In Proceedings of the 2008 IEEE International Conference on e-Business Engineering, Xi'an, China, 22–24 October 2008; pp. 563–567.
12. Ivanov, D. BioMEMS Sensor Systems for Bacterial Infection Detection. *Biodrugs* **2006**, *20*, 351–356. [CrossRef] [PubMed]
13. Mitsakakis, K.; Tserepi, A.; Gizeli, E. SAW device integrated with microfluidics for array-type biosensing. *Microelectron. Eng.* **2009**, *86*, 1416–1418. [CrossRef]
14. Nomura, T.; Yasuda, T. Surface acoustic wave liquid sensors based on one-port resonator. *Jpn. J. Appl. Phys.* **1993**, *32*, 2372. [CrossRef]
15. Morozumi, K.; Kadota, M.; Hayashi, S. Characteristics of BGS wave resonators using ceramic substrates and their applications. In Proceedings of the 1996 IEEE Ultrasonics Symposium, San Antonio, TX, USA , 3–6 November 1996; Volume 1, pp. 81–86.
16. Smagin, N.; Djoumi, L.; Herth, E.; Vanotti, M.; Fall, D.; Blondeau-Patissier, V.; Duquennoy, M.; Ouaftouh, M. Fast time-domain laser Doppler vibrometry characterization of surface acoustic waves devices. *Sens. Actuators A Phys.* **2017**, *264*, 96–106. [CrossRef]
17. Yuan, W.; Zhao, J.; Zhang, D.; Zhong, Z. Measurement of Surface Acoustic Wave Using Air Coupled Transducer And Laser Doppler Vibrometer. In Proceedings of the 21st International Conference on Composite Materials, Xian, China, 20–25 August 2017.
18. Nakamura, K. Shear-horizontal piezoelectric surface acoustic waves. *Jpn. J. Appl. Phys.* **2007**, *46*, 4421. [CrossRef]
19. Bleustein, J.L. A new surface wave in piezoelectric materials. *Appl. Phys. Lett.* **1968**, *13*, 412–413. [CrossRef]
20. Gulyaev, Y.V. Electroacoustic surface waves in solids. *ZhETF Pisma Redaktsiiu* **1969**, *9*, 63.
21. Pop, F.V.; Kochhar, A.S.; Vidal-Álvarez, G.; Piazza, G. Investigation of electromechanical coupling and quality factor of X-cut lithium niobate laterally vibrating resonators operating around 400 MHz. *J. Microelectromech. Syst.* **2018**, *27*, 407–413. [CrossRef]
22. Zhang, S.; Lu, R.; Zhou, H.; Link, S.; Yang, Y.; Li, Z.; Huang, K.; Ou, X.; Gong, S. Surface acoustic wave devices using lithium niobate on silicon carbide. *IEEE Trans. Microw. Theory Tech.* **2020**, *68*, 3653–3666. [CrossRef]
23. Avramov, I. 1 GHz low loss coupled resonator filter using surface skimming bulk waves and Bleustein-Gulyaev waves. *Electron. Lett.* **1991**, *27*, 414–415. [CrossRef]
24. Miyamoto, A.; Wakana, S.; Ito, A. Novel optical observation technique for shear horizontal wave in SAW resonators on 42/spl deg/YX-cut lithium tantalate. In Proceedings of the 2002 IEEE Ultrasonics Symposium, 2002, Munich, Germany, 8–11 October 2002; Volume 1, pp. 89–92.
25. Kim, M.G.; Jo, K.; Kwon, H.S.; Jang, W.; Park, Y.; Lee, J.H. Fiber-optic laser Doppler vibrometer to dynamically measure MEMS actuator with in-plane motion. *J. Microelectromech. Syst.* **2009**, *18*, 1365–1370.
26. Arabi, M.; Gopanchuk, M.; Abdel-Rahman, E.; Yavuz, M. Measurement of In-Plane Motions in MEMS. *Sensors* **2020**, *20*, 3594. [CrossRef] [PubMed]
27. Plessky, V.; Wang, W.; Wang, H.; Wu, H.; Shui, Y. P2M-4 Optimization of STW Resonator by Using FEM/BEM. In Proceedings of the 2006 IEEE Ultrasonics Symposium, Vancouver, BC, Canada, 2–6 October 2006; pp. 1863–1865.
28. Mimura, M.; Ajima, D.; Konoma, C.; Murase, T. Small sized band 20 SAW duplexer using low acoustic velocity Rayleigh SAW on LiNbO 3 substrate. In Proceedings of the 2017 IEEE International Ultrasonics Symposium (IUS), Washington, DC, USA, 6–9 September 2017; pp. 1–4.
29. Kowarsch, R.; Ochs, W.; Giesen, M.; Dräbenstedt, A.; Winter, M.; Rembe, C. Real-time 3D vibration measurements in microstructures. In *Optical Micro-and Nanometrology IV*; International Society for Optics and Photonics: Bellingham, WA, USA, 2012; Volume 8430, p. 84300C.
30. Chiba, Y.; Ebihara, T.; Mizutani, K.; Wakatsuki, N. Measurement of Love wave propagation characteristics along elastic substrate and viscoelastic surface layer. In Proceedings of the 37th Symposium on Ultrasonic Electronics (USE2016), Busan, Korea, 16–18 November 2016; Volume 37, p. 2P2-2.
31. Ayers, J.; Apetre, N.; Ruzzene, M.; Sabra, K. Measurement of Lamb wave polarization using a one-dimensional scanning laser vibrometer (L). *J. Acoust. Soc. Am.* **2011**, *129*, 585–588. [CrossRef] [PubMed]
32. Schmidt, T.E.; Tyson, J.; Galanulis, K.; Revilock, D.M.; Melis, M.E. Full-field dynamic deformation and strain measurements using high-speed digital cameras. In Proceedings of the 26th International Congress on High-Speed Photography and Photonics, Alexandria, VA, USA, 20–24 September 2004; Volume 5580, pp. 174–185.
33. Ehrhardt, D.A.; Allen, M.S.; Yang, S.; Beberniss, T.J. Full-field linear and nonlinear measurements using continuous-scan laser doppler vibrometry and high speed three-dimensional digital image correlation. *Mech. Syst. Signal Process.* **2017**, *86*, 82–97. [CrossRef]
34. Guo, F.; Sun, R. Propagation of Bleustein–Gulyaev wave in 6mm piezoelectric materials loaded with viscous liquid. *Int. J. Solids Struct.* **2008**, *45*, 3699–3710. [CrossRef]
35. Guo, F.; Wang, G.; Rogerson, G. Inverse determination of liquid viscosity by means of the Bleustein–Gulyaev wave. *Int. J. Solids Struct.* **2012**, *49*, 2115–2120. [CrossRef]
36. Kiełczyński, P.; Szalewski, M.; Balcerzak, A.; Rostocki, A.; Tefelski, D. Application of SH surface acoustic waves for measuring the viscosity of liquids in function of pressure and temperature. *Ultrasonics* **2011**, *51*, 921–924. [CrossRef] [PubMed]
37. Zaitsev, B.; Kuznetsova, I.; Joshi, S.; Borodina, I. Acoustic waves in piezoelectric plates bordered with viscous and conductive liquid. *Ultrasonics* **2001**, *39*, 45–50. [CrossRef]
38. Collet, B.; Destrade, M.; Maugin, G.A. Bleustein–Gulyaev waves in some functionally graded materials. *Eur. J. Mech. A Solids* **2006**, *25*, 695–706. [CrossRef]

39. Elhady, A.; Basha, M.; Abdel-Rahman, E. Tunable Bleustein-Gulyaev Permittivity Sensors. In *New Trends in Nonlinear Dynamics*; Springer: Cham, Switzerland, 2020; pp. 3–11.
40. Kadota, M.; Ago, J.; Horiuchi, H.; Morii, H. Transversely coupled resonator filters utilizing reflection of Bleustein-Gulyaev-Shimizu wave at free edges of substrate. *Jpn. J. Appl. Phys.* **2000**, *39*, 3045. [CrossRef]
41. Butt, Z.; Anjum, Z.; Sultan, A.; Qayyum, F.; Ali, H.M.K.; Mehmood, S. Investigation of electrical properties & mechanical quality factor of piezoelectric material (PZT-4A). *J. Electr. Eng. Technol.* **2017**, *12*, 846–851.